Cell Tissue Res
DOI 10.1007/s00441-012-1413-9

REGULAR ARTICLE

Differential uptake of MRI contrast agents indicates charge-selective blood-brain interface in the crayfish

Adriane G. Otopalik · Jane Shin · Barbara S. Beltz · David C. Sandeman · Nancy H. Kolodny

Received: 4 October 2011 / Accepted: 19 March 2012

Abstract This study provides a new perspective on the long-standing problem of the nature of the decapod crustacean blood-brain interface. Previous studies of crustacean blood-brain interface permeability have relied on invasive histological, immunohistochemical and electrophysiological techniques, indicating a leaky non-selective blood-brain barrier. The present investigation involves the use of magnetic resonance imaging (MRI), a method for non-invasive longitudinal tracking of tracers in real-time. Differential uptake rates of two molecularly distinct MRI contrast agents, namely manganese (Mn(II)) and Magnevist® (Gd-DTPA), were observed and quantified in the crayfish, *Cherax destructor*. Contrast agents were injected into the pericardium and uptake was observed with longitudinal MRI for approximately 14.5 h. Mn(II) was taken up quickly into neural tissue (within 6.5 min), whereas Gd-DTPA was not taken up into neural tissue and was instead restricted to the intracerebral vasculature or excreted into nearby sinuses. Our results provide evidence for a charge-selective intracerebral blood-brain interface in the crustacean nervous system, a structural characteristic once considered too complex for a lower-order arthropod.

This work was supported by the Arnold and Mabel Beckman Foundation, the Howard Hughes Medical Institute and the National Science Foundation [grants IOS-1121345 (to B.S.B.) and DBI-0116263 (to N.H.K.)].

A. G. Otopalik · B. S. Beltz · D. C. Sandeman
Neuroscience Program, Wellesley College,
Wellesley MA 02481, USA

J. Shin · N. H. Kolodny (✉)
Chemistry Department, Wellesley College,
106 Central Street,
Wellesley MA 02481, USA
e-mail: nkolodny@wellesley.edu

Published online: 19 April 2012

Keywords Crustacean · Magnevist · Manganese · Magnetic resonance imaging · Blood-brain barrier

Introduction

The blood-brain barrier (BBB) homeostatically regulates chemical flow between the bloodstream and neural tissue, playing an integral role in maintaining the necessary ionic environment for coordinated neural activity (Abbott et al. 1986; Abbott 2002). In vertebrate organisms, endothelial cells enclose intracerebral vasculature, forming tight junctions that restrict paracellular diffusion of polar molecules across this interface. Polar molecules must pass this barrier transcellularly, via specific membrane transporters (Bradbury 1993; Abbott 2002).

The presence of a BBB was confirmed in mammals by injecting trypan blue, a toluene derivative, into the rodent bloodstream (Goldmann 1909); all tissues except the brain and spinal cord were stained. On the other hand, when injected directly into the cerebrospinal fluid, trypan blue stained adjacent neural tissue relatively easily. This experiment suggested the presence of a structural barrier between the blood and brain in vertebrate organisms. Since Goldmann's seminal study, the BBB has been intensely investigated, with particular interest in its function, pathology and permeability as relevant to drug delivery.

Researchers have criticized the inefficiency and expense of rodent models for drug-delivery research, suggesting that lower-order model organisms might be more suitable in the early phases of drug development (Nielsen et al. 2011). Blood-brain interfaces have been identified in insects, crustaceans, some arachnids and cephalopod molluscs (Abbott and Pichon 1987). Thus, these invertebrates might serve as relatively inexpensive alternative model organisms in drug

discovery. For example, the grasshopper *Locusta migratoria* has been proposed as an alternative model for drug discovery, as its blood-brain interface appears to function similarly to the vertebrate BBB (Nielsen et al. 2011).

The blood-brain interface of the fruit fly, *Drosophila melanogaster*, has been particularly well characterized. Two glial layers with an outer collagenous neural lamella ensheath the *Drosophila* brain and restrict chemical flow between haemolymph and neural tissue (DeSalvo et al. 2011). Septate junctions between cells in the innermost glial layer of this interface allow the formation of a continuous sheet of glial cells. Permeability studies with ionic lanthanum (Juang and Carlson 1994) and differently sized dextran molecules (Stork et al. 2008) suggest that this interface is charge- and size-selective, respectively.

However, the *Drosophila* blood-brain interface is much simpler than the vertebrate BBB. The insect has an open circulatory system; haemolymph flows freely throughout body cavities, with the exception of a major dorsal vessel running the length of the organism. Oxygen is delivered to neural tissue via a network of air-filled tubes called tracheae (Pereanu et al. 2007), rather than via a complex network of intracerebral capillaries as observed in vertebrates. *Drosophila* has become the predominant invertebrate model for BBB study, despite this major anatomical difference, perhaps because of the abundance of molecular and genetic tools available for this organism (Pinsonneault et al. 2012; Daneman and Barres 2005).

The crustacean circulatory system and blood-brain interface is of a more controversial nature, a "case that is neither open nor closed" (McGaw 2005). Blood is pumped from the heart through a well-developed vasculature that services the major organs, including the nervous system. Blood then percolates from these organs into open sinuses that bathe tissues and from which the heart siphons newly oxygenated blood (Fig. 1). Most relevant to the present study, the dorsal artery carries blood from the heart into the cerebral ganglion, or brain, branching bilaterally and ultimately forming a complicated vascular network within the brain. Fine capillary networks terminate in "lacunae" in synaptic neuropils, from which the blood then flows out of the neural tissues (Figs. 1, 2) (Lane and Abbott 1975; Sandeman 1967; McGaw 2005). Whereas the respiratory tracheoles deliver oxygen within neural tissues in the insect, within crustacean ganglia a direct interface exists between the vasculature and the nervous system. Thus, although the crustacean blood-brain interface has been thought to closely resemble that of the insect, major differences are apparent.

A series of studies in the 1970s investigated the separation of blood and nerve tissue in the peripheral ganglia and central oesophageal connectives of decapod crustaceans (Kristensson et al. 1972; Abbott et al. 1975; Lane and Abbott 1977). These studies suggest two blood-brain interfaces at which resistance to chemical flow might occur (Fig. 1): (1) an interface between peripheral nerve tissue and the outer haemocoel and (2) the perineurium between central neural tissue and the outer haemocoel. Based on these studies, minimal resistance to chemical flow appears to occur at the peripheral interface. The second interface, separating the outer haemocoel from both the central oesophageal connectives and superficial neural tissue of the cerebral ganglion, is composed of a glial cell layer, the perineurium, enclosed by a collagenous sheath. Numerous tight junctions and few extracellular spaces can be found in the perineurium. Nevertheless, neither the collagenous extracellular material nor the minimal space between the perineurial cells results in an absolute barrier to ion flow at this interface (Abbott et al. 1975).

Few studies have probed the nature of the third blood-brain interface in crustaceans, i.e. that lying between the intracerebral capillaries and neural tissue (Fig. 1). Abbott (1970, 1971) has described a vast network of arterioles of mesodermal origin throughout the cerebral ganglion. Surrounding these vessels is a thick glial basement membrane with junctions between perivascular and interstitial neural glial and extracellular spaces no greater than 200 Å. These extracellular spaces are filled with polymeric material (Abbott 1970, 1971). However, other than restricting the flow of large colloidal molecules (larger than 160 Å) and increasing the diffusion path length, studies have suggested that this layer is an ineffective structural barrier. Thus, no crustacean intracerebral blood-brain barrier reminiscent of the ion-selective vertebrate blood-brain barrier seemed to exist. In this study, we have used contemporary technology to reconsider the possibility of an ion-selective intracerebral blood-brain interface in crustaceans.

The present study involves the use of magnetic resonance imaging (MRI) to demonstrate the presence of an ion-selective intracerebral blood-brain interface in the brain of the decapod crustacean (*Cherax destructor*). MRI offers the distinct advantage of being non-invasive and therefore amenable to longitudinal studies on a single animal over times ranging from minutes to weeks. By using MRI systems with powerful gradients, in-plane image resolution of 100 μm×100 μm or less can be obtained. Whereas the MR-image contrast caused by the different environments of water molecules in different tissues can be exploited to create useful images, the addition of exogenous molecules known as contrast agents can enhance the images in ways that reveal the properties of the system under study. Previous studies have employed cationic manganese (II) [Mn(II)] in investigations of crayfish anatomy and neural activity (Brinkley et al. 2005; Herberholz et al. 2004, 2011). Figure 2b, c shows MR images of the cerebral ganglion (brain) and

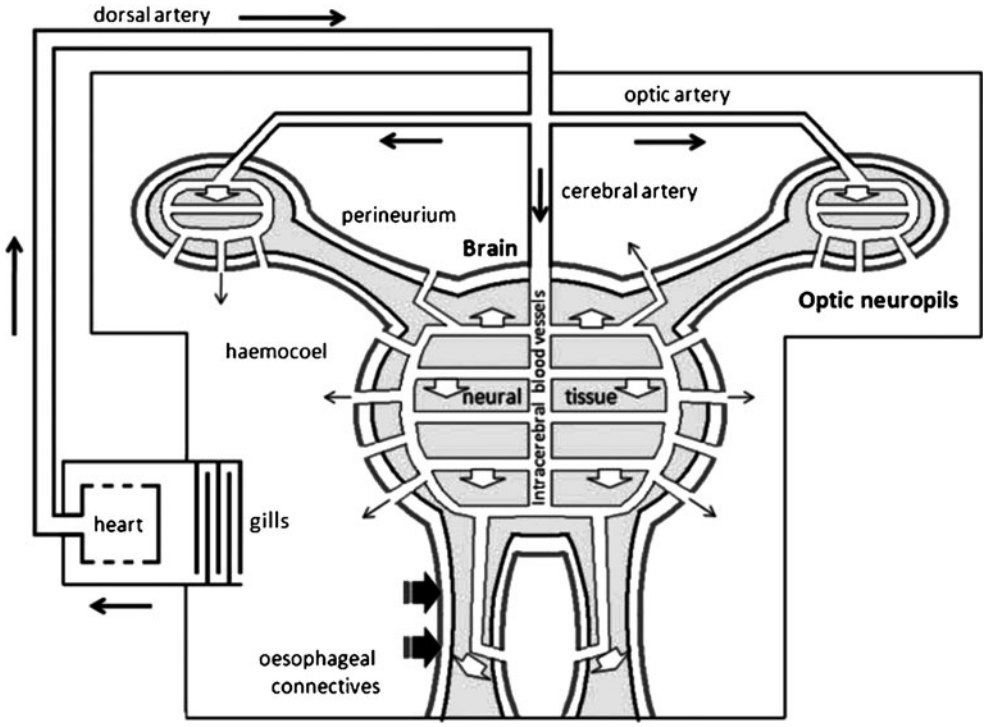

Fig. 1 Representation of the vascular circulation through the central nervous system in decapod crustaceans. Blood flow is unidirectional along arteries from the heart to the brain and optic neuropils (*thick arrows*). Within the neural tissue (*light grey*), the blood flows through intracerebral blood vessels. The blood exits through the cushion of glial cells and extracellular space (*white*) between the neural tissue of the brain and perineurium (*heavy line*), into the haemocoel (*thin arrows*) from which it passes through the gills and back to the heart. Previous studies suggest unrestricted flow from the intracerebral vasculature into neural tissue (*light grey*) in the brain and oesophageal connectives (*open broad arrows*) but restricted flow across the perineurium surrounding the brain and connectives (*filled broad arrows*)

optic ganglia of *C. destructor* after injection of Mn(II). The high resolution of these images reveals the detailed anatomy of the optic ganglia (Fig. 2c) and structures within the proto-, deutero- and tritocerebrum (see also Brinkley et al. 2005).

By using two molecularly distinct magnetic resonance contrast agents, namely Mn(II) and anionic Magnevist®, the latter being a gadolinium (Gd)-diethylenetriaminepentacetate (DTPA) complex (Fig. 3), qualitative and quantitative information about the differential uptake of agents with different sizes and charges can be obtained. Both Mn(II) and Magnevist® are paramagnetic contrast agents and enhance the MRI signal of (brighten) adjacent tissue in T1-weighted MR images. Mn(II) is an ionic probe with a weight of 54.9 amu, a double positive charge and an ionic diameter of 2.54 Å. Magnevist® is a molecular probe (Fig. 3) with a double negative charge, molecular weight of 938 amu and a molecular diameter of 8.2 Å (W.F. Coleman, personal communication). The differential uptake of these two probes confirms the presence of an ion-selective intracerebral blood-brain interface in the crayfish. The presence of this blood-brain interface suggests that the crayfish is a suitable model organism for examining the BBB. To our knowledge, this study is also the first in which the nature of an invertebrate blood-brain interface has been probed with a non-invasive technique.

Materials and methods

Animals Adult crayfish, *C. destructor*, were obtained commercially (Yabby Growers and Traders; Bulahdelah, NSW, Australia). The carapace length of the experimental animals was between 2.5 cm and 3.5 cm [n=3, Mn(II) experiments; n=5, Magnevist® experiments]. Animals were declawed at least 24 h prior to injection.

Dye injection into brain vasculature The dorsal artery supplying the crayfish brain was exposed, cannulated and perfused with chilled crayfish saline (CFS; 1 tsp/20 l $NaHCO_3$ and 1/8 tsp/20 l Equilibrium [Seachem Laboratories, Covington, Ga., USA], 19.5% K, 8.06% Ca, 2.41% Mg, 0.11% Fe, 0.06% Mn; pH 7.4) in a semi-intact brain preparation, as described by Sullivan et al. (2007) and Sandeman et al. (1995). The brain was initially perfused with CFS for several minutes to flush the haemolymph from the brain and to prevent the blockage of fine brain capillaries through clotting. Subsequently, the input to the cannula was switched to

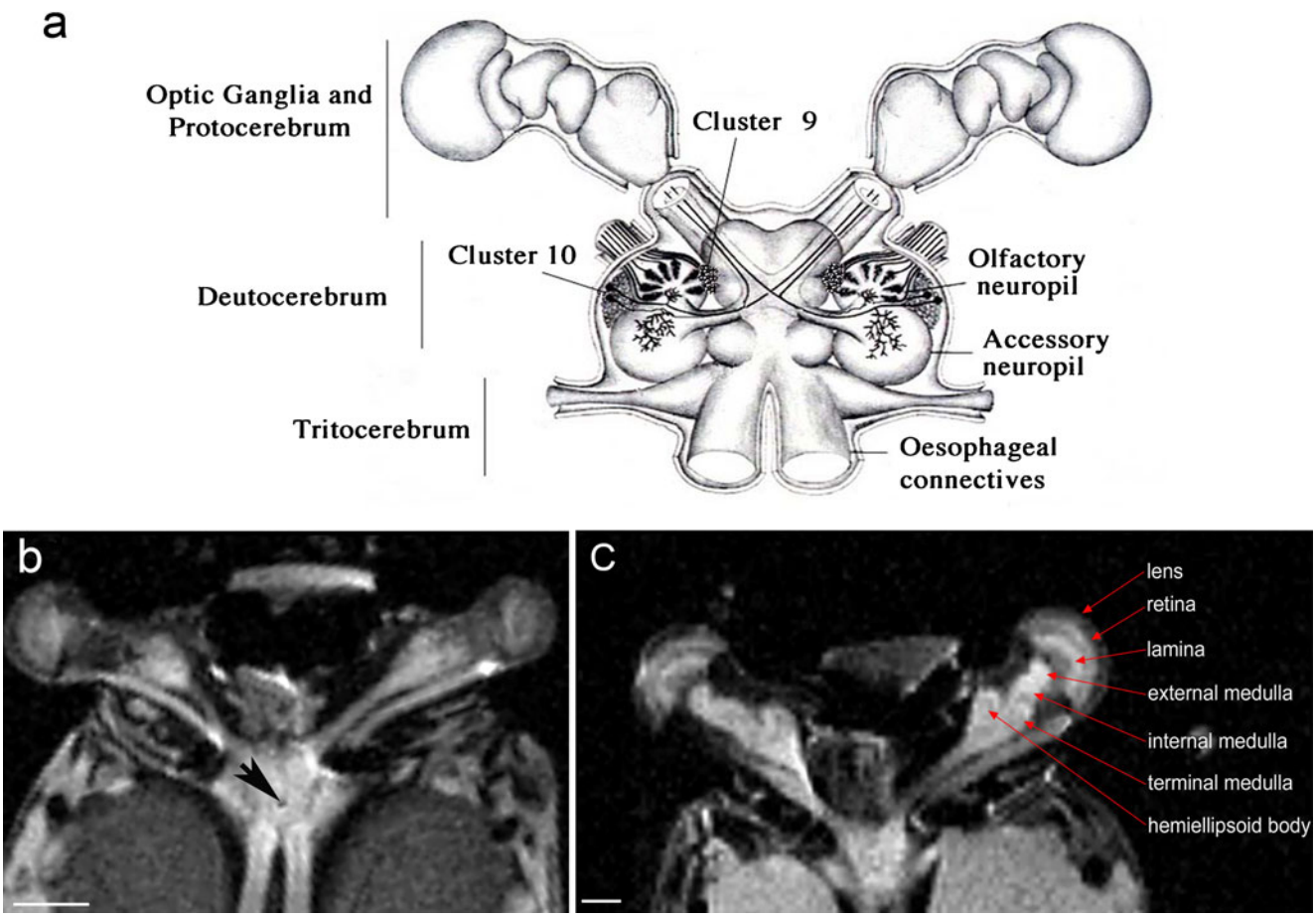

Fig. 2 **a** Representation of the cerebral ganglion (brain), including the lateral protocerebrum (eyestalks) and illustrating the major neuropil regions of the deutocerebrum. **b** Magnetic resonance (MR) image of a section through the brain in the dorsal-ventral plane, illustrating the oesophageal connectives, nerve roots and substructures of the brain and eyestalks (*arrow* insertion of the dorsal cerebral artery, which brings blood from the heart into the brain). **c** Individual neuropil regions in the lateral protocerebrum are revealed in this high-resolution manganese [Mn(II)]-enhanced image of the eyestalks of *Cherax destructor*. MR images acquired by using a T1-weighted multi-slice spin echo (MSME) protocol. *Bars* 1 mm (**b**, **c**). Figure adapted from Brinkley et al. (2005)

a sidearm containing a concentrated solution of dextran tetramethylrhodamine of 3,000 MW (Micro-Ruby; Molecular Probes), which was perfused into the brain over several minutes. The brain was then fixed overnight at 4°C in 4% paraformaldehyde. Following fixation, the brain was sectioned with a Vibratome (at a thickness of 100 μm), rinsed for 2 h in PBTx and mounted in Gel/mount™ (Biomeda, Foster City, Calif., USA). Sections were imaged with a Leica TCS SP5 confocal microscope equipped with 488-nm argon and 561- and 633-nm diode lasers.

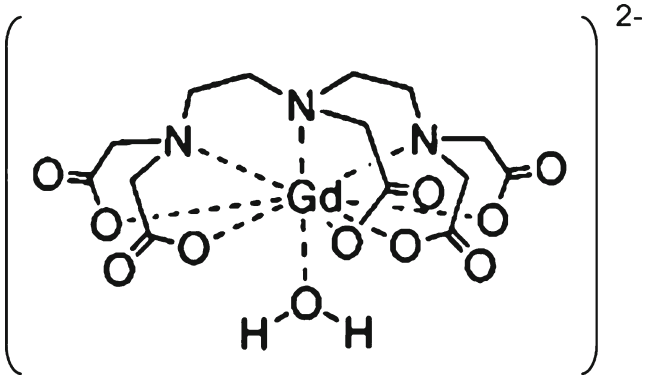

Fig. 3 Structure of Magnevist®, a gadolinium-diethylenetriamine pentaacetic acid (Gd-DTPA) complex. Figure adapted from Caravan et al. (1999)

Contrast agents Prior to imaging, a solution containing either $MnCl_2$ or gadopentate dimeglumine (Magnevist®) was injected ventrally into the pericardium (Fig. 4a, inset). For the Mn(II) contrast agent, 12 μl/g (crayfish weight) $MnCl_2$ solution [160 mM Mn(II) saline solution (2.4 g NaCl, 0.08 g KCl, 0.04 g $NaHCO_3$, 6.33 g $MnCl_2 \cdot 4H_2O$; Sigma)] in 200 ml CFS was injected (concentrations adapted from Silva et al. 2004). For Magnevist® (Berlex Laboratories, Wayne, N.J., USA; 469.01 mg/ml gadopentate dimeglumine, 0.99 mg/ml meglumine, 0.40 mg/ml diethylenetriamine pentaacetic acid), 0.2 μl/g (crayfish weight) was injected.

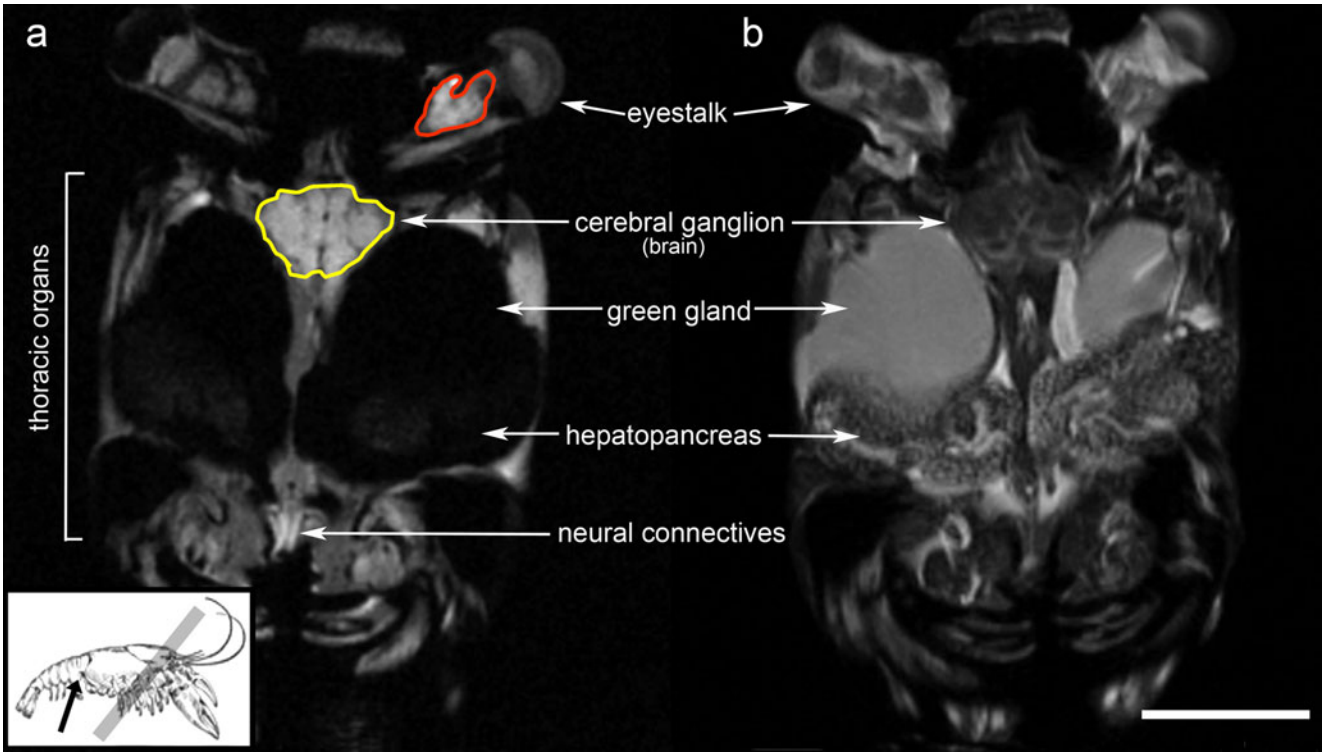

Fig. 4 T1-weighted MR images of *C. destructor*, illustrating the distinctive intensities of structures in the crayfish thorax when injected with different contrast agents. **a** Crayfish injected in the pericardium (*arrow*, *inset*). MR image obtained at the orientation indicated (*inset*, *diagonal grey bar*), such that the optic ganglia and cerebral ganglion (brain) could be imaged in the same slice. Image acquired 6.5 h post-injection of Mn(II). **b** Crayfish injected and imaged as in **a**. Image acquired 6.5 h post-injection of Magnevist®. Regions of interest: cerebral ganglion (delineated in *yellow*), optic ganglion (delineated in *red*). *Bar* 5 mm (**a**, **b**)

MR imaging MR images were acquired by using a Bruker Avance DRX 400 MHz NMR spectrometer with a 9.4 T vertical wide-bore magnet, actively shielded gradients of 2.4 G/(cm A) and a micro-imaging accessory. Following injection of either of the contrast agents, animals were wrapped in an ACE™ bandage and damp paper towel to reduce movement and placed in a 50-ml Corning® plastic tube. The tube was then positioned in the 30-mm birdcage volume coil (Bruker Instruments, Billerica, Mass., USA) of the MRI probe. The probe was inserted into the vertical bore magnet and MR images were acquired at 20°C.

Scout images were produced by using the Bruker ParaVision 4.0.2 tripilot pulse sequence, RARE (fast spin echo) (Field of view [FOV]=4 cm, Matrix [MTX]=256, slice thickness=0.50 mm, number of averages [N_{avg}]=1, Repetition Time/Time to Echo [TR/TE]=3112.5 ms/60.8 ms, Acquisition Time [TA]=1.39 min). By using the scout images, MRI slices of ensuing images were aligned in the plane of the ventral surface of the head (Fig. 4a, inset), in order to align the plane of the MRI scans symmetrically and consistently (Brinkley et al. 2005).

T1-weighted images were obtained by using Bruker ParaVision 4.0.2. Employment of a macromanager tool allowed for computer-monitored sequential scans post-injection. Nine T1-weighted scans were acquired during the first hour post-injection (msme_bio, FOV=2 cm, MTX=256, slice thickness=0.5 mm, N_{avg}=4, TR/TE=305.1 ms/10.2 ms, TA=6.5 min). Following the first hour, 16 additional higher-resolution T1-weighted scans were acquired each hour, with N_{avg}=24 and a TA of 31 min 14 s.

Data analysis Analyze 10.0 (AnalyzeDirect, Mayo Clinic, Overland Park, Kansas, USA) 3D voxel registration was used to align and normalize the thresholds of all scans to the first scan in a sequence. The region of interest tool was used to obtain mean regional intensities of the cerebral ganglion and optic nerve across sequential scans. Differences in values were considered statistically significant at $p \leq 0.05$.

Results

Injection of either contrast agent, Mn(II) or Magnevist®, revealed neural architecture in T1-weighted MR images (Fig. 4a, b, respectively). Longitudinal MR images also indicated the differential uptake rates of the two agents (Fig. 5).

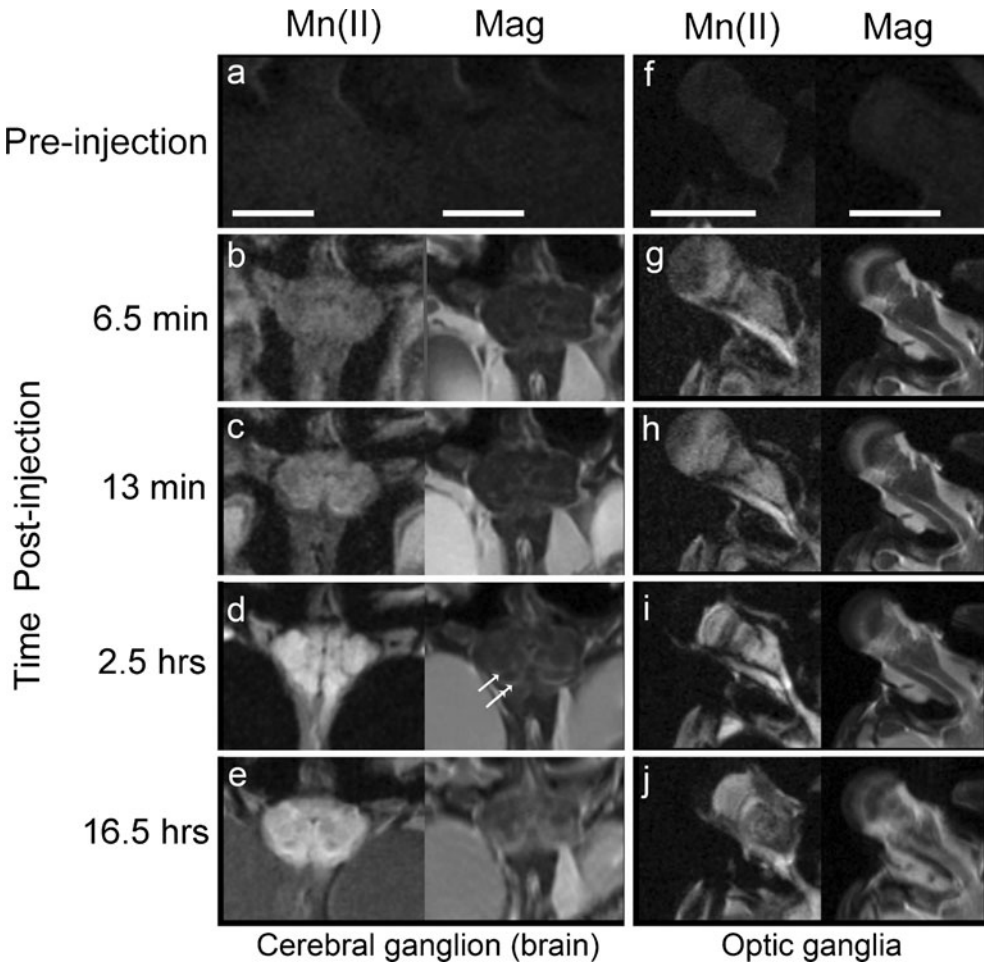

Fig. 5 Series of T1-weighted MR images illustrating the uptake of Mn(II) and Magnevist® (*Mag*) in the cerebral ganglion (**a-e**) and optic ganglia (**f-j**). Images were acquired pre-injection (**a**, **f**) and at 6.5 min (**b**, **g**), 13 min (**c**, **h**), 2.5 h (**d**, **i**) and 16.5 h (**e**, **j**) post-injection (*arrows* in **d** *right* point to the collection of Magnevist® at caudal boundaries of accessory lobe and antennal neuropils). *Bars* 2.5 mm (**a-e**), 5 mm (**f-j**)

Differential uptake of Mn(II) and Magnevist® into neural tissue

Mn(II) was taken up preferentially into neural tissue, as indicated by the brightening of the cerebral and optic ganglia relative to other tissue types (Fig. 4a). Contrast attributable to Mn(II) was notable in the brain by 6.5 min following injection (Fig. 5b, left) and then became increasingly intense up to 16.5 h (Fig. 5e, left). The increase in intensity of brain tissues over time and the delineation of specific synaptic and cell body regions suggested that the Mn(II) moved from the capillaries in the brain and optic ganglia into the neuropils in which the synapses are located.

T1-weighted images indicated that Magnevist®, unlike Mn (II), remained in fluid-filled body cavities (e.g. surrounding the optic ganglia) or was taken up and excreted via the green glands (Fig. 4b), which were more intense compared with most other tissues. Visualization of the cerebral ganglion in MR images also suggested resistance to Magnevist® movement across the interface between the intracerebral capillaries and neural tissue (Fig. 4b). Magnevist® collected in spaces at the caudal boundaries of the accessory lobe and antennal neuropils (Figs. 4b; 5d and e, right; 6a). However, rather than diffusing into the synaptic neuropils of the cerebral ganglion, Magnevist® remained in the intracerebral vasculature and presumably was eventually excreted from such intercellular spaces into the open circulatory sinus.

Magnevist®-enhanced MR images of the cerebral ganglion (Fig. 6a) showed contrast in regions similar to those observed in micrographs of a dextran (3,000 MW)-labelled cerebral ganglion (Fig. 6b). Like Magnevist®, dextran of this size did not enter neural tissue.

In the optic ganglia, increased contrast attributable to Mn (II) uptake in the retina and lamina was clearly visible at 2.5 h (Fig. 5i, left), illustrating features similar to the images in Fig. 2b and c but at a lower magnification and resolution. Magnevist® injection, however, appeared to increase the contrast at the margins of the optic nerve and did not penetrate the eye or enhance contrast in the optic neuropils (e.g. Fig. 5i, right).

Quantification of the different uptake rates in MR images

In addition to qualitative differences in the uptake of Mn(II) and Magnevist® illustrated in one-time-point MR images (Figs. 3, 4), quantitative differences in the rate of uptake across

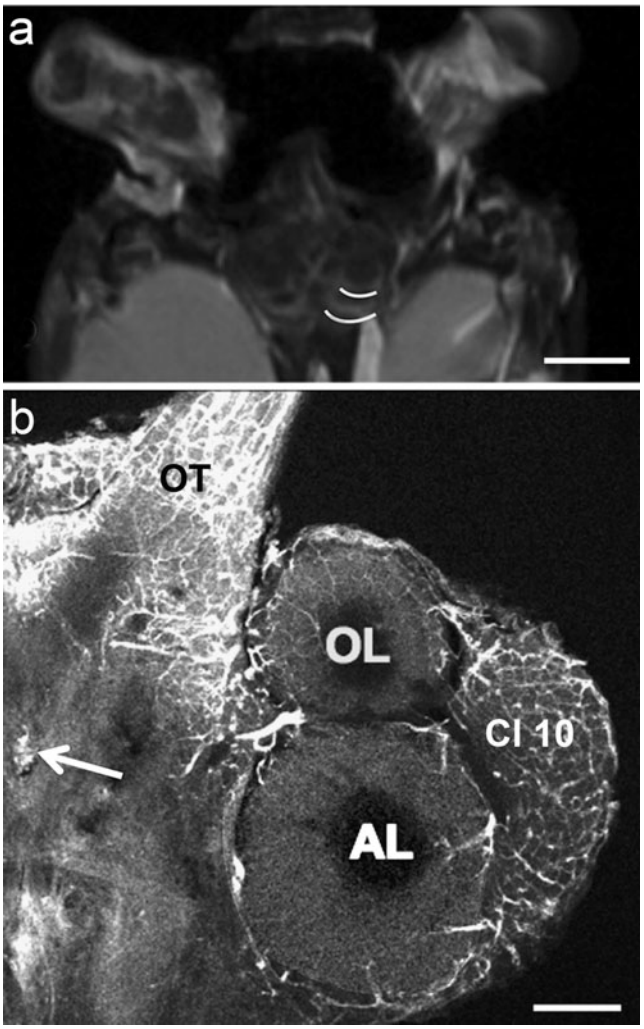

Fig. 6 Intracerebral vasculature in cerebral ganglion of *C. destructor*. **a** T1-weighted MR image following injection of Magnevist® (curved lines delineate brightened intensity of perimeters of the olfactory lobe and accessory lobe, which can be seen bilaterally. **b** Confocal micrograph of a right hemisphere labelled with dextran tetramethylrhodamine (*white*) showing intracerebral vasculature at higher magnification and the insertion point of the dorsal (cerebral) artery (*arrow*), which branches and forms a fine capillary network that is labelled in the optic tract (*OT*) and cell cluster 10 (*Cl 10*) containing olfactory projection neurons. Dextran-filled vasculature can also be seen encircling the olfactory lobe (*OL*) and accessory lobe (AL) and penetrating these synaptic regions in some areas. This is a dorsal section through the cerebral ganglion and therefore does not include the more ventral tritocerebral antennal lobes, which are located posterior to the accessory lobes. *Bars* 5000 μm (**a**), 200 μm (**b**)

the blood-brain interface were also observed in longitudinal imaging studies. Uptake of the two agents in neural tissue (the cerebral ganglion and optic ganglia) over time is shown in Fig. 5. A distinct increase in intensity occurred in the cerebral ganglion and optic ganglia after only 6.5 min following injection of Mn(II). Magnevist®, however, did not diffuse into neural tissue following injection and remained in the nearby vasculature or in fluid-filled cavities, as indicated by the slight increases in intensity in regions surrounding neural tissues after 2.5 h. These images illustrate the differential uptake of the two agents over time, with Mn(II) diffusing quickly across the blood-brain interface and into neurons and with Magnevist® remaining outside the neural tissue.

Uptake rates for the two agents were quantified by calculating the changes in the mean intensity over time in both the cerebral ganglion and optic ganglia in sequential MR images. Following injection of Mn(II), the cerebral ganglion intensity increased rapidly, peaked at approximately 3 h and then plateaued (Fig. 7a). Following injection of Magnevist®, however, the cerebral ganglion intensity remained low and relatively constant, suggesting minimal movement of Magnevist® across the blood-brain interface. Three days after injection, both contrast agents had been fully excreted from the animal (data not shown), as MR-image intensity of the brain had returned to baseline for both agents. Slopes of the change in mean regional MRI intensity with time, both initial (across 3 h following injection) and long-term (across ~14.5 h following injection), indicated a significant difference in the initial uptake of the contrast agents; following injection of Mn(II), the intensity of the signal in the cerebral ganglion increased at a rate four times that following injection of Magnevist® (Fig. 7b).

A similar uptake trend was observed for the optic ganglia (Fig. 8). A significantly higher initial mean intensity slope was seen in Mn(II)-enhanced images compared with those enhanced with Magnevist® (Fig. 8b). However, Mn(II) appeared to leave the optic ganglia relatively quickly, as suggested by the decay in intensity approximately 3 h following injection (Fig. 8a).

Discussion

Mn(II) easily crosses the intracerebral blood-brain interface

The present study demonstrates that Mn(II) experiences minimal resistance to crossing the blood-brain interface. This is consistent with previous findings. Manganese is an MRI contrast agent used for the study of brain anatomy, integration and function of neural circuits in vertebrates (Silva and Bock 2008). Earlier work comparing the flux of Ca(II) and Mn(II) ions suggests that, because of their similar ionic radii and charges, Mn(II) might act as a substitute for Ca(II) in vivo (Hunter et al. 1980), passing through calcium channels to enter neuronal terminals. Thus, unsurprisingly, Mn(II) is taken up preferentially by neural tissue, which requires a large amount of Ca(II) for its function. This phenomenon has also been employed by Herberholz et al. (2004) and Brinkley et al. (2005) in their use of Mn(II) to study neural anatomy in the crayfish brain.

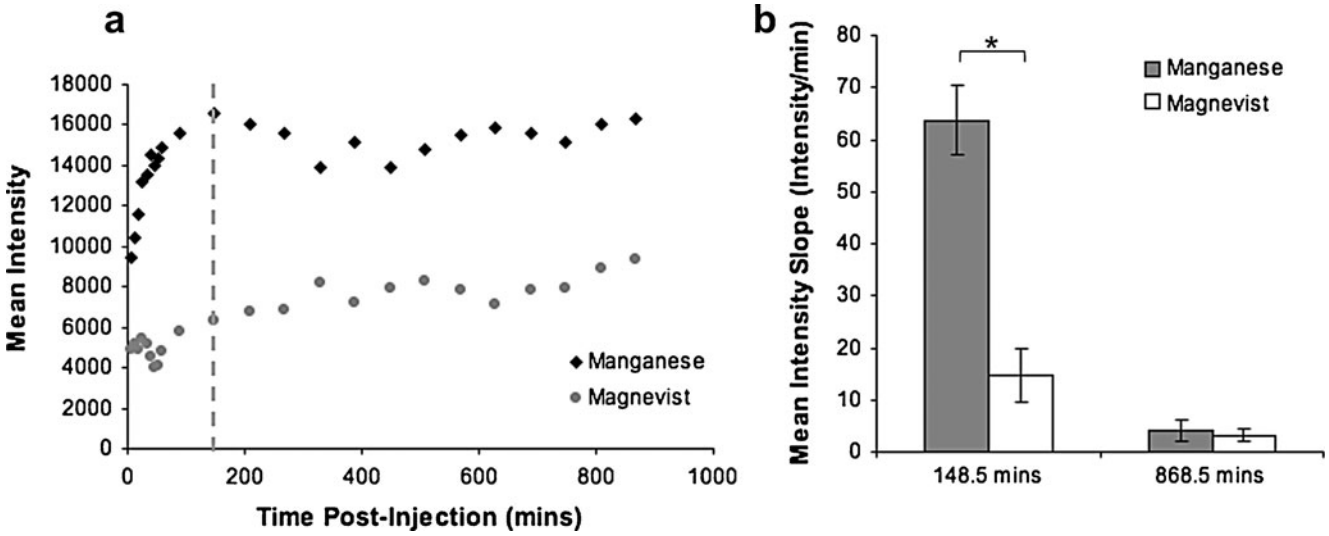

Fig. 7 MR-image intensity changes in the cerebral ganglion following injection of either Mn(II) or Magnevist®. **a** Example of the intensity change in the cerebral ganglion between 6.5 and 868.5 min post-injection of either Mn(II) or Magnevist® (n=1 for each contrast agent). **b** Mean slope of graphs of initial (up to 148.5 min) and long-term (between 148.5 and 868.5 min) intensity vs. time following injection of either Mn(II) (n=3) or Magnevist® (n=4) in the cerebral ganglion (*asterisk* indicates statistically different initial intensity slopes; t-test, df=2, 3, P=0.002). Initial slope was calculated as the change in mean intensity over the first eleven time points (*dashed vertical line* in **a**). *Error bars* denote standard error

The intensity decay in the optic ganglia at 3 h following Mn(II) injection is consistent with the anatomy of the animal. Afferent haemolymph circulation in the dorsal aorta branches three ways into the optic neuropils and cerebral ganglion (Sandeman 1967). Because the optic neuropils are relatively smaller than those in the brain, contrast agents might drain from the optic neuropil regions more rapidly. This results in faster intensity decay in MR images of optic ganglia relative to the cerebral ganglion.

Magnevist® does not flow across the intracerebral blood-brain interface

On the other hand, we have shown that Magnevist® is restricted from entering neural tissue, flowing only from intracerebral capillaries into external sinuses. Furthermore, the contrast shown in MR images following Magnevist® injection is consistent with that shown in micrographs following dextran injection. Dextran, paired with fluorescent markers,

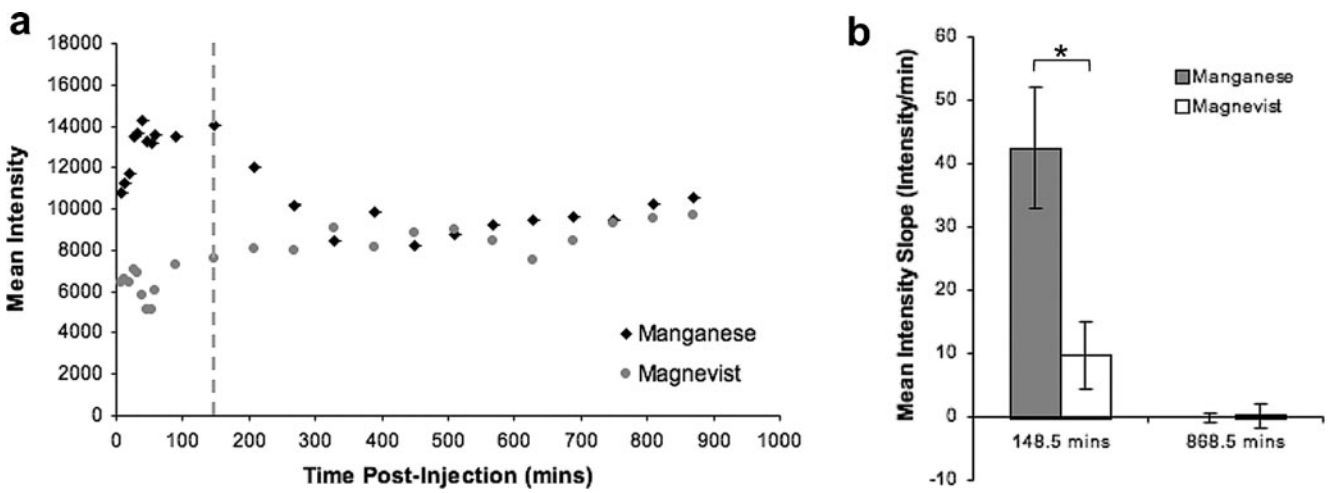

Fig. 8 Intensity changes in the optic nerve following injection of either Mn(II) or Magnevist®. **a** Example of the intensity change in the optic nerve between 6.5 min and 868.5 min post-injection of either Mn(II) or Magnevist® (n=1 for each contrast agent). **b** Mean initial (148.5 mins) and long-term (868.5 mins) intensity slopes following injection of either Mn(II) (n=3) or Magnevist® (n=4) in the optic nerve (*asterisk* denotes statistically different initial intensity slopes over the first 148.5 min; t-test, df=2, 3, P=0.02). Initial slope was calculated as change in mean intensity over the first eleven time points (*dashed vertical line* in **a**). *Error bars* denote standard error

Table 1 Summary of studies of blood-brain interface permeability in decapod crustaceans (*HRP* horseradish peroxidase, *n/a* not available)

Methods	Ion or molecule	Permeability	Tissue	Uptake half-time (min)	Ionic or molecular charge	Diameter (A)	Atomic weight (amus) or molecular weight (kDa)	Species	References
Incubation	Na^{+}	Yes	Central neural connectives	~2.91	+1	2.72	23 amu	*Carcinus maenas* and *Procambarus clarkii*	Abbott et al. 1975
	K^{+}	Yes	Central neural connectives	~193-8	+1	4.54	39 amu	*C. maenas* and *P. clarkii*	Abbott et al. 1975
	La^{3+}	No	Central neural connectives	n/a	+3	2.74	139 amu	*P. clarkii*	Lane and Abbott 1977[a]
Local Application Perfusion	HRP-VI	No	Brain	≤0.5	n/a	50-60	40 kDa	*A. astacas*	Kristensson et al. 1972[b]
	Dextran	No	Brain	n/a	Anionic	14	3 kDa	*P. clarkii*	Sullivan et al. 2007[c]
	^{131}l Serum albumin	No	Brain	n/a	Anionic	72	69 kDa	*C. maenas*	Abbott 1970
	Dextran	No	Brain	n/a	Anionic	167	110 kDa	*C. maenas*	Abbott 1970
	Ferritin	Yes	Brain	n/a	n/a (anionic, cationic, or neural)	100-120	450 kDa	*C.maenas*	Abbott 1972
	Trypan Blue	No	Brain	n/a	-4	300A	868 amu	*C. maenas*	Abbott 1970
Pericardial injection	Mn(II)	Yes	Brain	≤6.5	+2	2.54	54.9 amu	*C. destructor*	Otopalik et al. 2011
	Magnevist	No	Brain	—	-2	8.2[d]	938 amu	C. destructor	Otopalik et al. 2011

[a] Additional reference: Butt 1991

[b] Additional references include: Shivers 1976; Pino 1985

[c] Addition reference: supplier's information (Sigma-Aldrich)

[d] W.F. Coleman, personal communication

has long been used as a tracer in the study of circulation and vascular permeability in both vertebrates and invertebrates (Olsson et al. 1975; Thorball 1981; Wahl et al. 1985; Sullivan 2007). Like dextran-enhanced micrographs, Magnevist®-enhanced MR images show increased intensity in the intracerebral vasculature. Specifically, Magnevist® increases the intensity of the vasculature on the ventral side and capillary beds on the caudal boundary of the accessory and antennal lobes. A comparison of the images obtained from both Magnevist®-enhanced MRI and dextran-enhanced microscopy suggests no movement of Magnevist® across this intracerebral blood-brain interface.

Confirmation of earlier findings: anions restricted from neural tissue

Table 1 summarizes the previous and current findings regarding blood-brain permeability in decapod crustaceans. Several studies have characterized the perineurial barrier across central oesophageal connectives (Abbott et al. 1975; Lane and Abbott 1977), suggesting a size-selective barrier preventing the flow of larger ions (La^{3+}). However, these studies have not investigated the interface between the intracerebral vasculature and central neural tissue.

Other earlier studies have suggested the presence of an effective intracerebral structural barrier between crustacean blood and brain. Whereas the macromolecule ferritin crosses this interface with little resistance (Abbott 1972), the interface is relatively impermeable to cationic horseradish peroxidase (HRP; type VI; Kristensson et al. 1972). Likewise, Abbott (1970) has demonstrated the restriction of anionic serum albumin, dextran and trypan blue to the blood vasculature, implying the possibility of a charge-selective barrier restricting anionic molecules as small as 72 Å in diameter. Later work completed by Sullivan et al. (2007) using a much smaller isoform of dextran (14 Å) has demonstrated the restriction of an even smaller anionic molecule from crossing this intracerebral interface.

The present study with non-invasive technology to visualize the differential uptake of Mn(II) and Magnevist® in vivo and in real time complements the earlier findings by confirming the presence of a charge-selective intracerebral BBB. Cationic Mn(II), with its relatively small diameter and ionic weight, easily crosses this interface, whereas anionic Magnevist®, despite its relatively low molecular weight, is restricted from entering neural tissue. Our results clearly demonstrate the presence of a functional intracerebral BBB in the decapod crustacean *C. destructor*, a structural characteristic once considered too complex for a lower-order arthropod. Further, these features suggest that the crayfish blood-brain interface has similarities with the mammalian BBB but not with that of insects. For this reason, crustacean systems may provide a model superior to insects for drug-discovery testing.

Acknowledgements We gratefully acknowledge Amelia Bond, Olivia Hendrick, Jane Rodgers and Catherine Brinkley with regard to their early success in experiments with Mn(II) in crayfish. Additionally, we appreciate William Coleman's computational work in determining the molecular diameter of Magnevist®. We also thank Pat Carey and Jon Rose for animal maintenance and technological support, respectively and Jeanne Benton for extensive laboratory training and work on the figures accompanying the manuscript.

References

Abbott NJ (1970) Absence of blood-brain barrier in a crustacean, *Carcinus maenas* L. Nature 225:291–293

Abbott NJ (1971) The organization of the cerebral ganglion in the shore crab, *Carinus maenas*. II. The relation of intracerebral blood vessels to other brain elements. Z Zellforsch Mikrosk Anat 120:401–419

Abbott NJ (1972) Access of ferritin to the interstitial space of *Carcinus* brain from intracerebral blood vessels. Tissue Cell 4:99–104

Abbott NJ (2002) Astrocyte-endothelial interactions and blood-brain barrier permeability. J Anat 200:629–638

Abbott N, Pichon Y (1987) The glial blood-brain barrier of crutsacea and cephalopods: a review. J Physiol (Paris) 82:304–313

Abbott NJ, Moreton RB, Pichon Y (1975) Electrophysiological analysis of potassium and sodium movements in crustacean nervous system. J Exp Biol 63:85–115

Abbott NJ, Lane NJ, Bundgaard M (1986) The blood-brain interface in invertebrates. Ann N Y Acad Sci 481:20–42

Bradbury MW (1993) The blood-brain barrier. Exp Physiol 78:453–472

Brinkley C, Kolodny NH, Kohler S, Sandeman D, Beltz BS (2005) Magnetic resonance imaging at 9.4T as a tool for studying neural anatomy in non-vertebrates. J Neurosci Methods 146:124–132

Butt AM (1991) Modulation of a glial blood-brain barrier. Ann N Y Acad Sci 633:363–377

Caravan P, Ellison JJ, McMurry TJ, Lauffer RB (1999) Gadolinium (III) chelates as MRI contrast agents:structure, dynamics, and applications. Chem Rev 99:2293–2342

Daneman R, Barres B (2005) The blood-brain barrier—lessons from moody flies. Cell 123:9–12

DeSalvo M, Mayer N, Mayer F, Bainton R (2011) Physiologic and anatomic characterization of the brain surface glia barrier of *Drosophila*. Glia 59:1322–1340

Goldmann EE (1909) Die aussere and innere Sekretion des gesundes und kranken Organismus im Lichte der vitalen Farbung. Beitr Klin Chir 64:192–265

Herberholz J, Mims CJ, Zhang X, Hu X, Edwards DH (2004) Anatomy of a live invertebrate revealed by manganese-enhanced magnetic resonance imaging. J Exp Biol 207:4543–4550

Herberholz J, Mishra S, Uma D, Germann M, Edwards D, Potter K (2011) Non-invasive imaging of neuroanatomical structures and neural activation with high resolution MRI. Front Behav Neurosci 5:16

Hunter D, Komai H, Haworth R, Jackson M, Berkoff H (1980) Comparison of Ca^{2+}, Sr^{2+}, and Mn^{2+} fluxes in mitochondria of the perfused rat heart. Circ Res 47:721–727

Juang J, Carlson S (1994) Analog of vertebrate anionic sites in blood-brain interface of larval *Drosophila*. Cell Tissue Res 277:87–95

Kristensson K, Strömberg E, Elofsson R, Olsson Y (1972) Distribution of protein tracers in the nervous system of the crayfish (*Astacus*

astacus L.) following systemic and local application. J Neurocytol 1:35–48

Lane NJ, Abbott NJ (1975) The organization of the nervous system in the crayfish *Procambarus clarkii*, with emphasis on the blood-brain interface. Cell Tissue Res 156:173–187

Lane NJ, Abbott NJ (1977) Lanthanum penetration in crayfish nervous system: observations on intact and "desheathed" preparations. J Cell Sci 23:315–324

McGaw JJ (2005) The decapod crustacean circulatory system: a case that is neither open nor closed. Microsc Microanal 11:18–36

Nielsen P, Andersson O, Hansen S, Simonsen K, Andersson G (2011) Models for predicting blood-brain barrier permeation. Drug Discov Today 16:472–475

Olsson Y, Svensjo E, Arfors K, Hultstrom D (1975) Fluorescein labelled dextrans as tracers for vascular permeability studies in the nervous system. Acta Neuropathol 33:45–50

Otopalik AG, Dai YL (2011) Tracking cells from blood to brain: using MRI to study neurogenesis in the crayfish. The Ruhlman Conference, April 27, 2011. Wellesley College, Wellesley, pp 39–40

Pereanu W, Spindler S, Cruz L, Hartenstein V (2007) Traceal development in *Drosophila* brain is constrained by glial cells. Dev Biol 302:169–180

Pino RM (1985) Binding of fab-horseradish peroxidase conjugates by charge and not by immunospecificity. J Histochem Cytochem 33:55–58

Pinsonneault R, Mayer N, Mayer F, Tegegn N, Bainton R (2012) Novel models for studying the blood-brain and blood-eye barriers in *Drosophila*. Methods Mol Biol 686:357–369

Sandeman DC (1967) The vascular circulation of the brain, optic lobes, and thoracic ganglia of the crab *Carcinus*. Proc R Soc Lond [Biol] 168:82–90

Sandeman DC, Beltz BS, Sandeman R (1995) Crayfish brain interneurons that converge with serotonin giant cells in accessory lobe glomeruli. J Comp Neurol 352:263–279

Shivers RR (1976) Trans-glial channel-facilitated translocation of tracer protein across ventral nerve root sheaths of crayfish. Brain Res 108:47–58

Silva AC, Bock NA (2008) Manganese-enhanced MRI: an exceptional tool in translational neuroimaging. Schizophr Bull 34:595–604

Silva AC, Lee JH, Aoki I, Koretsky AP (2004) Manganese-enhanced magnetic resonance imaging (MEMRI): methodological and practical considerations. NMR Biomed 17:532–543

Stork T, Engelen D, Krudewig A, Silies M, Bainton R, Klämbt C (2008) Organization and function of the blood-brain barrier in *Drosophila*. J Neurosci 28:587–597

Sullivan JM, Benton JL, Sandeman DC, Beltz BS (2007) Adult neurogenesis: a common strategy across diverse species. J Comp Neurol 500:574–584

Thorball N (1981) FITC-dextran tracers in microcirculatory and permeability studies using combined fluorescence stereo microscopy, fluorescence light microscopy and electron microscopy. Histochemistry 71:209–223

Wahl M, Unterberg A, Baethmann A (1985) Intravital fluorescence microscopy for the study of blood-brain-barrier function. Int J Microcirc Clin Exp 4:3–18